Saulys, E. H. Willen, and S. J. Lindenbaum, Nucl. Instrum. Methods 108, 33 (1973).

[4] A possible background is from the reaction $\pi^- + p \to \Sigma^0(\to \Lambda + \gamma) + K^0$. However, the energy spectrum of γ rays from decaying 8-GeV/c Σ^0's is flat and ranges from 5 MeV to 1 GeV. Consequently the missing mass from the detected Λ would range from the K^0 (K^*) mass to $\gtrsim$1.5 GeV. Any background under the peaks will be subtracted in the fitting procedure.

[5] We have used a background which is linear in missing mass squared. Considering the statistics of this experiment, this simple function adequately represents the background under the K^* peaks. We estimate that our results would change by less than our overall systematic uncertainty of $\simeq 25\%$ by using nonlinear functional forms.

PHYSICAL REVIEW D VOLUME 10, NUMBER 9 1 NOVEMBER 1974

K^+-proton scattering from 200 to 600 MeV/c*

R. A. Burnstein, J. J. LeFebvre, D. V. Petersen, and H. A. Rubin
Illinois Institute of Technology, Chicago, Illinois 60616

T. B. Day, J. R. Fram,† R. G. Glasser, G. McClellan, B. Sechi-Zorn, and G. A. Snow
University of Maryland, College Park, Maryland 20742

(Received 18 June 1974)

The differential cross section for K^+p elastic scattering has been measured at several momenta in the interval 200–600 MeV/c within a hydrogen bubble chamber. The data have been fitted with a partial-wave analysis. We obtain solutions which are dominated over the entire momentum range by s-wave scattering, with constructive interference between the nuclear and Coulomb scattering. The effective-range approximation with only s waves yields a K^+p scattering length $a = -0.314 \pm 0.007$ F and an effective range $r_0 = 0.36 \pm 0.07$ F. The measured total inelastic cross section at 588 MeV/c is 11^{+9}_{-5} μb.

I. INTRODUCTION

Low-energy K^+-proton scattering information serves as an anchor point for the evaluation of K-nucleon dispersion relations and KYN coupling constants and for phase-shift analyses that search for exotic Z^* resonances in K-nucleon interactions. To improve this anchor point beyond the pioneering efforts of the Berkeley group[1,2] more than a decade ago, we have carried out a new investigation of K^+p differential cross sections in the momentum interval 200–600 MeV/c with improved statistics. Because of a suggestion by Carreras and Donnachie[3,4] that predominantly attractive s-wave scattering could give a good description of K^+p elastic scattering below 2.0 GeV/c, care has been taken to extend differential cross-section measurements far into the Coulomb-nuclear interference region.

The phase-shift solutions obtained using our data with an energy-independent phase-shift analysis[5] with pure s-wave nuclear scattering are satisfactory over the entire momentum interval, in agreement with the earlier results of Goldhaber *et al.*[1] In addition, we find that the K^+p strong interaction interferes constructively with Coulomb scattering and is therefore repulsive at these momenta. Using the effective-range approximation to fit the pure s-wave phase shifts gives the K^+p scattering length $a = -0.314 \pm 0.007$ F and the effective range $r_0 = 0.36 \pm 0.07$ F.

We have measured the total inelastic cross section at the upper end of the momentum range just 80 MeV/c above threshold.

II. EXPERIMENTAL METHOD

The experiment[6] was performed in the BNL-Columbia 30-inch hydrogen bubble chamber using the low-energy separated K^+ beam[7] at Brookhaven National Laboratory. The beam was transported at 614 MeV/c and moderated by means of copper absorbers upstream of the bubble chamber. The experiment consisted of 93 000 photographs divided up into four approximately equal runs at nominal K^+ momenta of 250, 360, 470, and 575 MeV/c. The distribution of beam momenta as measured at the interaction vertex for these runs is given in Fig. 1. The data at the lowest momentum were separated for the phase-shift analysis into two momentum regions, 110–200 MeV/c and 200–320 MeV/c. As indicated in Fig. 1, the mean momenta of the five sets of data are 178, 265, 351, 475, and 588 MeV/c.

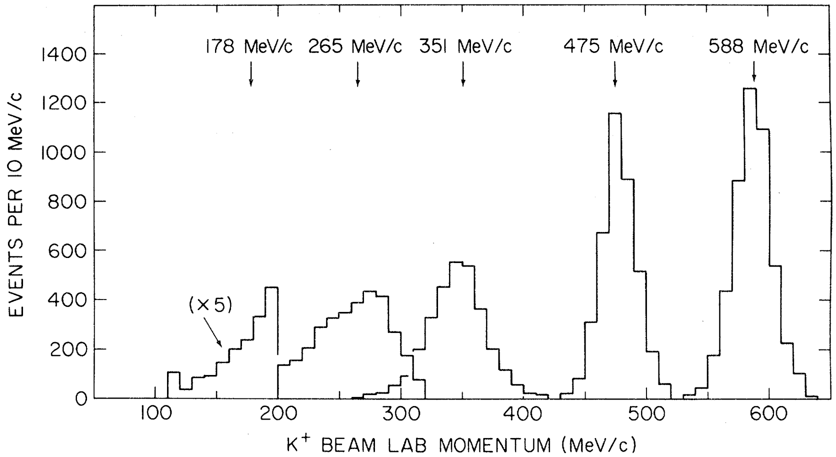

FIG. 1. The distribution of beam momenta as measured at the interaction vertex. The mean momentum is indicated for each data set.

A. Scanning and measurements

The film was scanned within a prescribed fiducial region for topologies with one, two, or three visible outgoing tracks. Elastic K^+p scatters produce the two-prong topology and also the one-prong topology when the recoil proton path length is too short to be observed. Only the Maryland sample at the three lower momenta was scanned for the one-prong topology. The K^+ τ decay ($K\to 3\pi$) produces the three-prong topology. One half of the Maryland film sample was double-scanned at all momenta. The IIT sample (limited to the upper three momenta) was completely double-scanned. Overall scanning efficiencies for the two- and three-prong topologies are listed in Table I.

No statistically significant dependence of the scanning efficiencies on the angles or momenta of outgoing tracks was found for the two- and three-prong events. On the other hand, the scanning efficiency for one-prong events was found to depend strongly on the scattering angle projected onto the scan table. The functional form shown in Table I gave a good fit to the scanning efficiency as a function of projected angle ψ, for $\psi > 4°$. Below $\psi = 4°$, the scanning efficiency is less than 0.50. To eliminate poorly scanned data, events with $\psi < 5°$(efficiency < 0.73) were not included in the final sample. This cut in ψ introduces a cut in the azimuthal angle corrected as discussed below.

Events were measured by means of manual and automatic (PEPR) measuring machines,[8] and the measurements were processed by the programs TVGP and SQUAW.[9]

B. Constants of the experiment

The various constants of importance in the experiment were determined in the following way. The liquid-hydrogen density ρ_H was determined by measuring the range of μ^+ from stopping-π^+ decays. The π^+ decays were obtained from a sample of τ decays ($K^+ \to \pi^+ + \pi^+ + \pi^-$) at all momenta. The mean μ^+ range was found to be 1.032 ± 0.004 cm, which implies $\rho_H = 0.0620 \pm 0.0006$ g/cm^3. The central magnetic field in the bubble chamber ($\overline{B}$) was 12.75 ± 0.13 kG based on magnet current readings during the run. An independent determination of the magnetic field yielded results within 1% of

TABLE I. Scanning efficiencies.

	178 MeV/c	265 MeV/c	351 MeV/c	475 MeV/c	588 MeV/c
τ-decay scanning efficiency	0.959 ± 0.005	0.959 ± 0.005	0.952 ± 0.009	0.994 ± 0.002	0.988 ± 0.004
Two-prong K^+p scanning efficiency	0.990 ± 0.003	0.990 ± 0.003	0.990 ± 0.003	0.994 ± 0.003	0.993 ± 0.003
One-prong K^+p scanning efficiency	$\epsilon = 0.9733\left[1 - \frac{2.424}{(\psi - 1.903)^2}\right]$ ψ = projected angle $\geq 5°$ (in degrees)			...	...

TABLE II. Data and K^+p differential cross sections.

p_{lab} (MeV/c)	$\cos\theta_{\text{c.m.}}$ interval	$\langle\cos\theta_{\text{c.m.}}\rangle_{\text{av}}$	Observed number of scatters	Scanning efficiency	Azimuthal acceptance	Pion subtraction (No. of events)	$d\sigma/d\Omega$ (mb/sr)
178	−1.0 to −0.6	−0.800	34	0.99	1.0	⋯	1.10 ± 0.18
	−0.6 to −0.2	−0.400	29	0.99	1.0	⋯	0.93 ± 0.18
	−0.2 to 0.2	0.003	35	0.99	1.0	⋯	1.13 ± 0.19
	0.2 to 0.6	0.408	40	0.99	0.97	⋯	1.32 ± 0.21
	0.6 to 0.8	0.707	28	0.98	0.90	⋯	2.03 ± 0.37
	0.8 to 0.9	0.856	22	0.98	0.85	⋯	3.33 ± 0.69
	0.90 to 0.97	0.946	34	0.96	0.71	⋯	9.05 ± 1.6
	0.97 to 0.985	0.979	27	0.91	0.52	⋯	49.1 ± 8.8
		(observed τ count = 131)				(fitted τ count = 139)	
265	−1.0 to −0.8	−0.900	238	0.99	1.00	⋯	1.117 ± 0.072
	−0.8 to −0.6	−0.700	230	0.99	1.00	⋯	1.079 ± 0.072
	−0.6 to −0.4	−0.500	217	0.99	1.00	⋯	1.018 ± 0.073
	−0.4 to −0.2	−0.300	270	0.99	1.00	⋯	1.267 ± 0.073
	−0.2 to 0.0	−0.100	240	0.99	1.00	⋯	1.126 ± 0.073
	0.0 to 0.2	0.100	253	0.99	1.00	⋯	1.187 ± 0.074
	0.2 to 0.4	0.301	252	0.99	1.00	⋯	1.183 ± 0.075
	0.4 to 0.6	0.501	260	0.99	1.00	⋯	1.222 ± 0.077
	0.6 to 0.8	0.704	311	0.97	0.985	⋯	1.513 ± 0.084
	0.8 to 0.9	0.853	153	0.97	0.84	⋯	1.73 ± 0.15
	0.9 to 0.96	0.935	184	0.96	0.75	⋯	3.93 ± 0.28
	0.96 to 0.985	0.976	137	0.93	0.56	⋯	9.77 ± 0.90
		(observed τ count = 1290)				(fitted τ count = 1278)	
351	−1.0 to −0.8	−0.900	338	0.99	1.00	⋯	0.963 ± 0.054
	−0.8 to −0.6	−0.700	366	0.99	1.00	⋯	1.043 ± 0.054
	−0.6 to −0.4	−0.500	351	0.99	1.00	⋯	1.006 ± 0.054
	−0.4 to −0.2	−0.300	368	0.99	1.00	⋯	1.051 ± 0.054
	−0.2 to 0.0	−0.100	380	0.99	1.00	⋯	1.085 ± 0.054
	0.0 to 0.2	0.100	391	0.99	1.00	⋯	1.117 ± 0.054
	0.2 to 0.4	0.300	354	0.99	1.00	⋯	1.011 ± 0.055
	0.4 to 0.6	0.501	422	0.99	1.00	⋯	1.206 ± 0.056
	0.6 to 0.8	0.703	359	0.99	1.00	⋯	1.027 ± 0.059
	0.8 to 0.925	0.867	296	0.98	0.87	⋯	1.580 ± 0.092
		(observed τ count = 1589)				(fitted τ count = 1573)	
	0.925 to 0.960	0.944	86	0.965	0.73	⋯	2.78 ± 0.29
	0.960 to 0.985	0.975	73	0.92	0.56	⋯	4.55 ± 0.61
		(observed τ count = 1112)				(fitted τ count = 1105)	
475	−1.0 to −0.8	−0.900	387	0.994	1.00	0.0	1.043 ± 0.053
	−0.8 to −0.6	−0.700	348	0.994	1.00	0.0	0.937 ± 0.053
	−0.6 to −0.4	−0.500	418	0.994	1.00	0.0	1.126 ± 0.053
	−0.4 to −0.2	−0.300	387	0.994	1.00	0.0	1.043 ± 0.053
	−0.2 to 0.0	−0.100	389	0.994	1.00	0.4	1.047 ± 0.053
	0.0 to 0.4	0.201	798	0.994	1.00	6.0	1.066 ± 0.038
	0.4 to 0.6	0.501	400	0.994	1.00	0.0	1.078 ± 0.054
	0.6 to 0.8	0.702	423	0.994	0.97	2.6	1.168 ± 0.056
	0.8 to 0.95	0.882	341	0.994	0.88	9.4	1.391 ± 0.081
		(observed τ count = 1255)				(fitted τ count = 1251)	
588	−1.0 to −0.8	−0.900	500	0.993	1.00	0.0	1.086 ± 0.047
	−0.8 to −0.6	−0.700	475	0.993	1.00	0.0	1.031 ± 0.047
	−0.6 to −0.4	−0.500	494	0.993	1.00	0.0	1.072 ± 0.047
	−0.4 to −0.2	−0.300	444	0.993	1.00	1.8	0.960 ± 0.047
	−0.2 to 0.0	−0.100	444	0.993	1.00	3.5	0.956 ± 0.047
	0.0 to 0.4	0.200	957	0.993	1.00	0.9	1.038 ± 0.034
	0.4 to 0.6	0.500	503	0.993	1.00	0.0	1.092 ± 0.048
	0.6 to 0.8	0.701	484	0.993	1.00	6.4	1.056 ± 0.049
	0.8 to 0.95	0.880	411	0.955	0.915	14.5	1.303 ± 0.069
		(observed τ count = 1248)				(fitted τ count = 1246)	

this nominal value. The check consisted of a comparison of π^+ momenta as determined from the range measurements with π^+ momenta as determined solely from curvature measurements in the magnetic field for a sample of stopping π^+ from τ decays.

C. Path length

The K^+ path length was measured for each of the different momentum intervals from the number of events which fitted the τ-decay hypothesis at that momentum. The path length in centimeters is given by

$$L=(p/M)\times ct\times N_\tau/B\,,$$

where p and M are the momentum and mass of the decaying K^+ expressed in MeV/c and MeV/c^2, respectively; $ct=370.8\pm0.8$ cm is the K^+ lifetime[10]; N_τ is the number of τ decays; and $B=0.0558\pm0.0003$ is the τ-decay branching ratio.[10] The observed number of τ decays is used as a parameter in the phase-shift analysis of the differential cross section. The observed and fitted numbers are included in Table II for each momentum interval. Table II is a compilation of angular distributions, data corrections, and differential cross sections, as discussed below.

D. Corrections

There is a small contamination of pions in the beam. These pions do not affect the K^+ path-length determination, which is based on a count of the number of τ decays. At momenta of 351 MeV/c and below, π^+ elastic scatters are easily eliminated at the scan table since the π^+ ionization is less than half of the K^+ ionization at the same momentum. At 475 and 588 MeV/c, a certain fraction of π^+p two-prong scatter events contaminate the K^+p scatter sample by appearing to satisfy the kinematics of K^+p scattering. At these momenta the π^+ contamination is not generally separable by ionization estimates. From a sample of events which are unambiguously determined to be π^+p scatters, we find that the pion contamination in the beam has a significantly broader distribution in momentum, azimuth, and dip than the K^+ beam. For this reason, restricting the spread of the beam parameters reduced π^+ contamination to less than 1% with a relatively small loss of K^+. For consistency these same restrictions are applied to the τ-decay sample. The small remaining contamination of π^+p events occurs only at the two angular intervals at which there is a kinematic ambiguity between π^+p and K^+p fits. One class of ambiguity occurs when the proton of the π^+p scatter is misinterpreted as a scattered K^+ meson while the pion is misinterpreted as a proton; the other occurs when the meson scattering angle is small so that the kinematics is insensitive to its mass. The corrections for this effect are included in Table II.

There is a loss of events for orientations of the scattering plane such that the projected scattering angle seen by the scanner is very small. The distribution of the azimuthal angle, ϕ, of the scattering plane rotated about the beam direction must be uniform by symmetry considerations. We have used this fact to correct the two-prong distributions at forward angles and to correct for one-prong events cut out when the projected scattering angle is $\leq 5°$, as noted earlier. The corrections are listed in Table II under the heading "Azimuthal acceptance." The number listed for each $\cos\theta_{\text{c.m.}}$ interval is the estimated fraction of events observed.

A small fraction of events were unmeasurable because tracks were obscured, or because outgoing tracks decayed or were scattered too near the vertex. A correction is applied to the number of observed K^+p scatters to account for these unmeasurable events. This correction has been included in the differential cross sections shown in Table II and amounts to 0.4% at 588 MeV/c, 0.6% at 475 MeV/c, 0.5% at 351 MeV/c, 0.3% at 265 MeV/c, and 0.3% at 178 MeV/c.

The two-prong K^+p angular distributions were cut off at $\cos\theta_{\text{c.m.}}=0.95$ because at that angle the proton recoils are ≤ 1 mm long and therefore their detection efficiency is substantially reduced. The missing events should appear as one-prong K^+p scatters and were recorded and measured at the three lower momenta, thus extending the angular distributions to $\cos\theta_{\text{c.m.}}=0.985$. At 477 MeV/$c$ and 588 MeV/c one-prong scatters become confused with the larger sample of one-prong K^+ decays since the decay angles and ionization differences are not sufficient to easily identify the outgoing particle.

III. RESULTS AND ANALYSIS OF DATA

A. Angular distributions

Figure 2 presents the K^+p differential cross sections. Table II contains a listing of these data. The errors listed are mainly statistical but also include estimated uncertainties in the corrections and scanning efficiencies.

B. Energy-independent phase-shift analysis

The data were analyzed using a phase-shift expansion[5]:

$$\frac{d\sigma}{d\Omega}=(1/k^2)\,|kf_C(\theta)+T(0,\tfrac{1}{2})+[T(1,\tfrac{1}{2})+2T(1,\tfrac{3}{2})]\cos\theta\,|^2+(1/k^2)\,|T(1,\tfrac{1}{2})-T(1,\tfrac{3}{2})|^2\sin^2\theta\,,$$

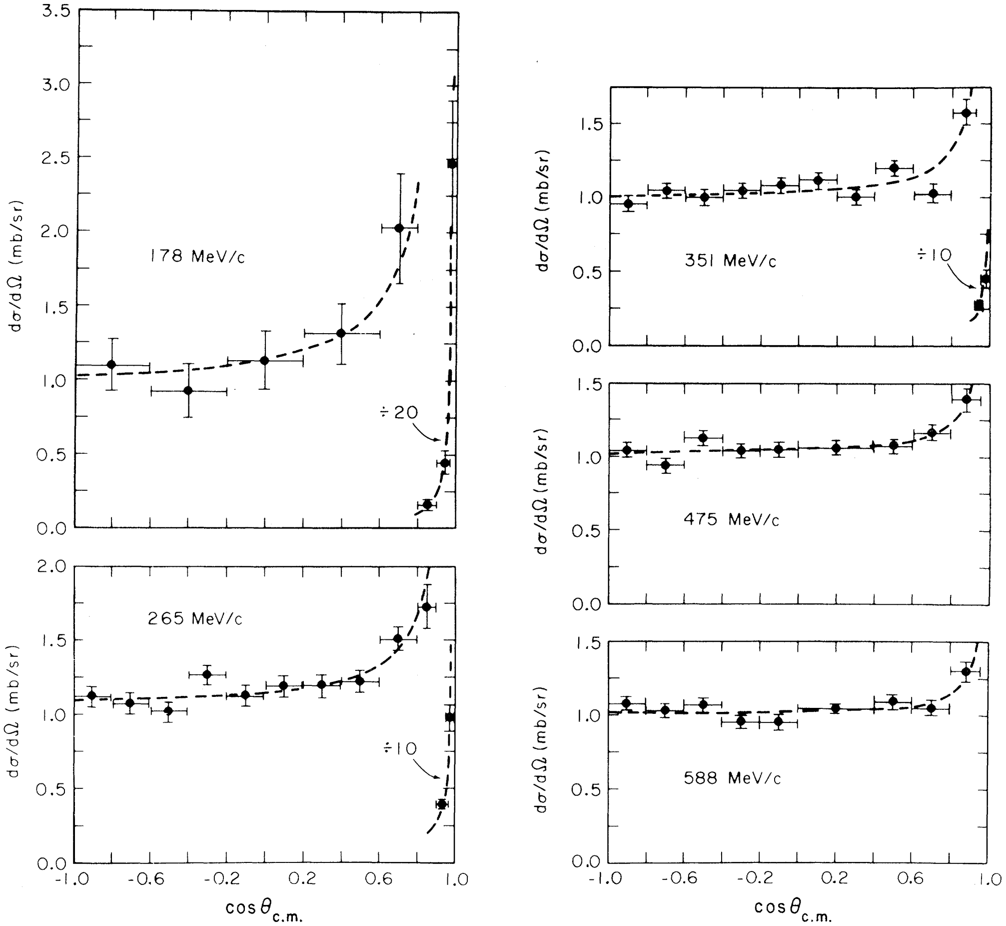

FIG. 2. Differential cross sections for K^+p elastic scattering. The curves are fits obtained with negative s-wave phase shifts for the nuclear scattering amplitude.

where the Coulomb amplitude is

$$f_C(\theta) = \frac{-\alpha}{2k\sin^2(\theta/2)} \exp[-i\alpha \ln \sin^2(\theta/2) + 2i\sigma_0],$$

with

$$\alpha = \frac{e^2}{\hbar V_{\mathrm{rel}}}, \quad \sigma_0 = \arg\Gamma(1+i\alpha),$$

and the nuclear amplitude for orbital angular momentum l and total angular momentum j is

$$T(l,j) = (1/2i)[\exp(2i\delta_{l,j}) - 1].$$

The nonrelativistic Coulomb amplitude $f_C(\theta)$ is a good approximation for K^+ momenta up to 600 MeV/c, if relativistic kinematics is used to obtain the relative velocity V_{rel} of the incoming K^+ and the target proton.[11] The quantity k is the wave number, θ is the scattering angle, and $\delta_{l,j}$ is the phase shift.

The phase-shift analysis includes the full Coulomb contribution, but has only real phase shifts. The inelastic threshold is at 509 MeV/c, so that at our lowest momenta the phase shifts must be real. At 588 MeV/c the K^+p inelastic cross section is about 0.1% of the total cross section (see below). Thus, the inelasticity is negligible and the phase shift may still be taken as real. The Coulomb amplitude, f_C, interferes with the spin-non-flip nuclear amplitudes. Since we obtain good fits without any d or higher waves, we omit them in our analysis.

The phase-shift solutions were obtained from a minimization procedure. The parameters were varied to minimize χ^2 given by

$$\chi^2 = \sum_{i=1}^{n+1} \left| \left(\frac{N_{\mathrm{expt}} - N_{\mathrm{theo}}}{\Delta N} \right)_i \right|^2,$$

where N_{expt} is the observed number of events in each $\cos\theta_{\mathrm{c.m.}}$ interval for the first n terms and it is the observed number of τ decays for the $n+1$ term. N_{theo} is the expected number of events calculated from the phase shifts for the first n terms

TABLE III. Phase-shift solutions.

p_{lab} (MeV/c)	χ^2/N_d	Confidence level	$\delta(s_{1/2})$ (degrees)	$\delta(p_{1/2})$ (degrees)	$\delta(p_{3/2})$ (degrees)	Fitted path length (km)
178	2.1/7	0.95	−10.08 ± 0.81			3.39 ± 0.35
	2.0/6	0.92	−10.16 ± 0.85	−0.25 ± 0.81		3.35 ± 0.37
	2.0/5	0.84	−10.17 ± 0.85	−0.09 ± 3.24	−0.09 ± 1.64	3.35 ± 0.37
	275.4/7	0.00	+13.58 ± 0.35			6.26 ± 0.44
	152.1/6	0.00	+9.04 ± 0.46	+5.00 ± 0.41		9.78 ± 0.84
	141.7/5	0.00	+9.64 ± 0.33	+1.71 ± 1.01	+1.71 ± 0.51	10.91 ± 0.96
	156.0/6	0.00	+1.43 ± 0.18	+7.24 ± 0.32		12.50 ± 1.35
	1.9/6	0.93	−0.04 ± 0.77	−11.33 ± 0.83		3.31 ± 0.35
	1.5/5	0.92	−0.10 ± 0.79	+3.38 ± 0.74	−7.71 ± 0.63	3.24 ± 0.36
	144.4/5	0.00	+2.80 ± 0.40	−3.80 ± 0.40	+5.60 ± 0.34	8.95 ± 1.14
265	13.1/11	0.29	−15.96 ± 0.35			46.5 ± 1.6
	13.0/10	0.23	−15.93 ± 0.36	+0.11 ± 0.32		46.7 ± 1.6
	12.7/9	0.18	−15.71 ± 0.59	−2.00 ± 2.08	+1.07 ± 1.08	46.8 ± 1.6
	12.7/9	0.18	−15.71 ± 0.59	+2.10 ± 2.13	−0.98 ± 1.03	46.8 ± 1.6
	2113.6/11	0.00	+23.24 ± 0.28			45.9 ± 1.1
	1587.6/10	0.00	+17.44 ± 0.27	+6.20 ± 0.20		66.3 ± 1.9
	1523.9/9	0.00	+17.39 ± 0.24	+2.22 ± 0.54	+2.22 ± 0.28	72.0 ± 2.2
	1951.9/10	0.00	+2.56 ± 0.13	+10.50 ± 0.09		142.7 ± 3.0
	13.3/10	0.21	+0.20 ± 0.31	−16.81 ± 0.36		46.5 ± 1.6
	12.8/9	0.17	+0.21 ± 0.31	+5.93 ± 0.29	−10.98 ± 0.25	46.7 ± 1.6
	1218.7/9	0.00	+5.03 ± 0.20	−1.46 ± 0.22	−10.23 ± 0.17	87.0 ± 3.0
351	28.7/21	0.12	−20.22 ± 0.37			76.1 ± 1.8
	27.9/20	0.11	−20.18 ± 0.37	+0.30 ± 0.34		76.3 ± 1.8
	24.0/19	0.20	−19.23 ± 0.60	−4.50 ± 1.14	+2.50 ± 0.63	76.7 ± 1.8
	24.0/19	0.20	−19.23 ± 0.60	+4.85 ± 1.22	−2.15 ± 0.56	76.7 ± 1.8
	1161.4/21	0.00	+25.31 ± 0.46			73.6 ± 1.9
	1018.6/20	0.00	+23.63 ± 0.77	+4.16 ± 0.40		80.1 ± 3.5
	923.6/20	0.00	+3.71 ± 0.31	+22.07 ± 0.48		84.8 ± 2.5
	28.4/20	0.10	+0.34 ± 0.33	−20.90 ± 0.37		76.2 ± 1.8
	24.0/19	0.20	+0.38 ± 0.33	+7.84 ± 0.32	−13.41 ± 0.25	76.7 ± 1.8
	811.5/19	0.00	+6.57 ± 0.34	−3.79 ± 0.35	+18.12 ± 0.27	64.8 ± 1.5
475	6.9/8	0.55	−27.51 ± 0.64			80.2 ± 3.0
	6.9/7	0.44	−27.50 ± 0.64	+0.10 ± 0.46		80.3 ± 3.0
	6.4/6	0.38	−27.03 ± 0.92	−3.57 ± 2.53	+1.94 ± 1.41	80.4 ± 3.0
	6.4/6	0.38	−27.03 ± 0.92	+3.78 ± 2.73	−1.73 ± 1.21	80.4 ± 3.0
	121.0/8	0.00	+30.96 ± 0.63			76.0 ± 2.7
	59.1/7	0.00	+30.19 ± 0.64	+3.41 ± 0.42		78.4 ± 2.9
	56.4/6	0.00	+30.32 ± 0.64	+1.21 ± 1.41	+1.21 ± 0.72	78.5 ± 2.9
	58.4/7	0.00	+3.42 ± 0.42	+29.64 ± 0.64		78.5 ± 2.9
	6.9/7	0.44	+0.12 ± 0.45	−28.10 ± 0.64		80.3 ± 3.0
	6.4/6	0.38	+0.16 ± 0.45	+10.39 ± 0.49	−17.89 ± 0.41	80.4 ± 3.0
	32.1/6	0.00	+3.48 ± 0.41	−8.46 ± 0.48	−19.42 ± 0.40	79.6 ± 3.0
588	9.0/8	0.34	−33.51 ± 0.77			99.6 ± 3.6
	7.7/7	0.36	−33.41 ± 0.78	+0.57 ± 0.51		99.9 ± 3.6
	7.7/6	0.26	−33.42 ± 0.78	+0.19 ± 3.11	+0.19 ± 1.56	99.9 ± 3.6
	81.9/8	0.00	+36.52 ± 0.77			95.9 ± 3.4
	55.2/7	0.00	+36.06 ± 0.78	+2.56 ± 0.48		97.6 ± 3.5
	53.7/6	0.00	+36.13 ± 0.78	+0.92 ± 1.46	+0.92 ± 0.75	97.7 ± 3.5
	54.8/7	0.00	+2.56 ± 0.48	+35.55 ± 0.78		97.7 ± 3.5
	7.7/7	0.36	+0.58 ± 0.50	−33.97 ± 0.78		99.9 ± 3.7
	6.1/6	0.42	+0.50 ± 0.51	+12.06 ± 0.58	−21.55 ± 0.47	99.6 ± 3.6
	19.1/6	0.01	+2.80 ± 0.46	−10.24 ± 0.57	+22.93 ± 0.46	99.0 ± 3.6

and it is the fitted number of τ decays for the $n+1$ term. The various scanning efficiencies and corrections discussed earlier are included in the calculation of N_{theo}. The error ΔN includes the Poisson error $(N_{\text{theo}})^{1/2}$ and the uncertainties in the scanning efficiencies and other corrections.

Because of the $n+1$ term in χ^2, the overall normalization of $d\sigma/d\Omega$ is a free parameter in the fit. The normalization is determined mainly by the observed number of τ decays, but is also affected by the K^+p data at small angles since the Coulomb part of the cross section is known. The observed and fitted number of τ decays are included in Table II. The differential cross sections in Table II were calculated from the observed number of elastic scatters and from the fitted number of τ decays. The errors quoted do not include the uncertainty in the number of τ decays. This uncertainty in the overall normalization of $d\sigma/d\Omega$ is indicated by the uncertainty in the path lengths listed in Table III. These path lengths are calculated from the fitted number of τ decays.

C. Results of phase-shift analysis

At each momentum we have searched for solutions with various combinations of s- and p-wave strong-interaction amplitudes using both positive and negative phase shifts. The solutions obtained are presented in Table III. For each solution we have listed χ^2, the number of degrees of freedom N_d, the confidence level, and the fitted path length. The errors are computed as the amount by which a parameter must be changed to give a change of 1 in χ^2.

In all cases a good solution was found using only an s-wave amplitude with a negative phase shift. These solutions are plotted in Fig. 2. The addition of a small $p_{1/2}$ amplitude $T(1, \frac{1}{2})$ results in a $p_{1/2}$ phase shift consistent with zero in all cases. This result reflects the observed isotropy of the measured differential cross section, since the p-wave nonflip amplitude $[T(1, \frac{1}{2}) + 2T(1, \frac{3}{2})] \cos\theta$ would interfere with an s-wave amplitude to give a nonisotropic differential cross section.

When both $p_{1/2}$ and $p_{3/2}$ amplitudes are used with a negative s-wave phase shift, solutions are obtained which keep the p-wave nonflip amplitude close to zero but allow a small spin-flip p-wave amplitude, i.e., $\delta(p_{1/2}) \simeq -2\delta(p_{3/2})$. The spin-flip amplitude does not interfere with the larger s-wave and Coulomb amplitudes, so it remains a small contribution to the differential cross section. These phase-shift solutions are plotted in Fig. 3 as a function of momentum. When there was a choice between a negative and a positive $p_{1/2}$ phase shift, we have chosen the negative value as indicated[12,13] by the analysis of previous data combined with dispersion-relation constraints.

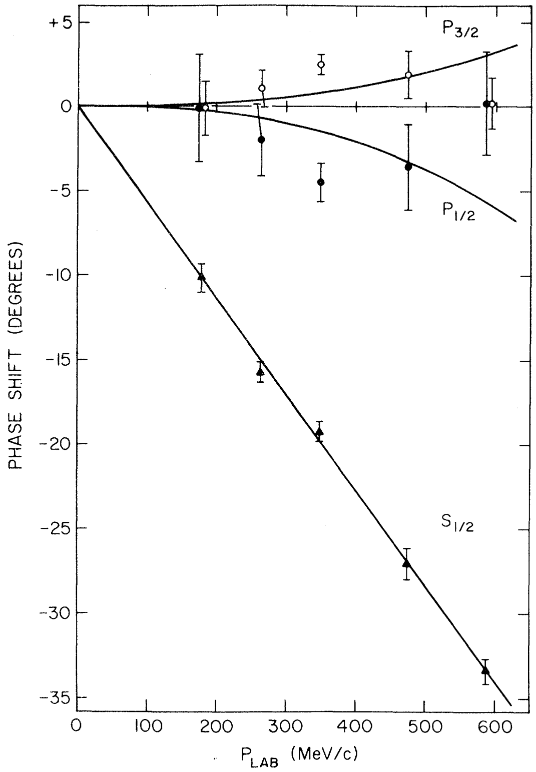

FIG. 3. Phase shifts as a function of momentum for the solutions which included all s and p waves. The curves are the effective-range fits to each partial wave.

Only at 351 MeV/c did the addition of p waves improve the fit to the differential cross section. Even here the increase in confidence level from 0.12 to 0.20 is not very significant. We conclude that a pure s-wave strong-interaction amplitude adequately describes all our elastic scattering data.

An s-wave amplitude with a negative (positive) phase shift interferes constructively (destructively) with the repulsive Coulomb amplitude. A comparison of pure s-wave fits to the differential cross section with positive and negative phase shifts is shown in Fig. 4 at 265 and 588 MeV/c. Since the normalization of the differential cross section is effectively a parameter in the fitting procedure, we have plotted the number of observed events per steradian rather than the differential cross section for the comparison. At 265 MeV/c (similarly at 178 and 351 MeV/c) measurements in the Coulomb scattering region make it dramatically apparent that the strong interaction interferes constructively with the repulsive Coulomb force. Even at 588 MeV/c (similarly at 475 MeV/c), where one-prong events were not measured, the

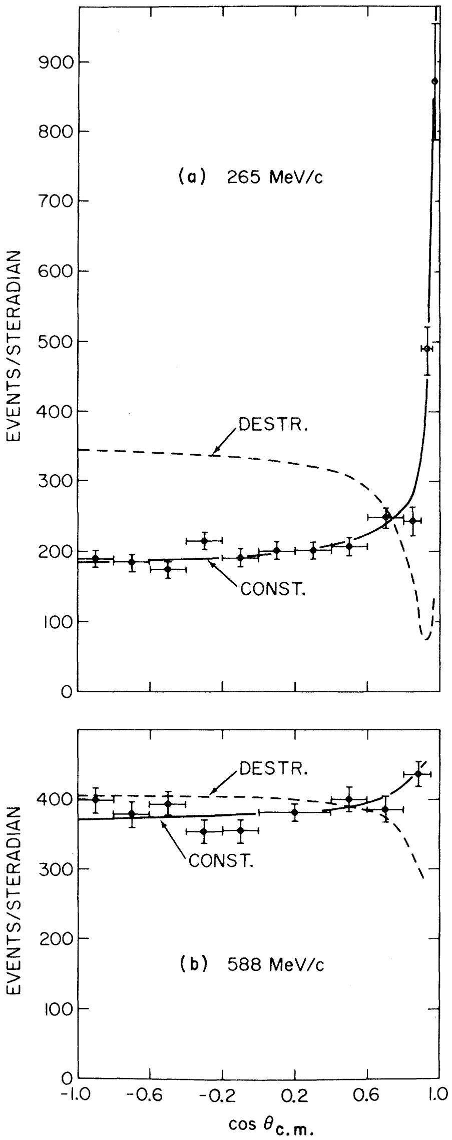

FIG. 4. The K^+p scattering angular distribution at (a) 265 MeV/c and (b) 588 MeV/c. The solid fitted curves are for constructive nuclear-Coulomb interference [$\delta(s_{1/2}) < 0$] and the dashed fitted curves are for destructive interference [$\delta(s_{1/2}) > 0$].

constructive interference is readily apparent. We conclude that the s-wave phase shift is negative over the momentum range 178–588 MeV/c.

There are additional solutions listed in Table III which fit the observed isotropic K^+p angular distribution with good confidence level. They are due to the Minami ambiguity and the Fermi-Yang ambiguity. The first involves dominant $p_{1/2}$-wave scattering with $\delta(p_{1/2}) < 0$ and the second is a mixture of $p_{1/2}$- and $p_{3/2}$-wave scattering with $\delta(p_{1/2}) \simeq -0.5\delta(p_{3/2}) > 0$. Both solutions produce isotropic scattering and constructive Coulomb-nuclear interference with a negligible s-wave contribution. While these solutions cannot in principle be ruled out at a particular momentum without nucleon polarization measurements, they are unlikely since the fitted phase shifts display a linear dependence on momentum rather than the k^3 dependence expected near threshold.

TABLE IV. Total cross sections.

K^+ laboratory momentum (MeV/c)	Experimental $\sigma_{(\text{Nuclear + Coulomb})}$ $\cos\theta_{\text{c.m.}} < 0.85$ (mb)	$\delta(s_{1/2})$ fitted (degrees)	σ_{Nuclear} (mb)
178	14.8 ± 2.0	-10.1 ± 0.8	11.4 ± 1.8
265	13.9 ± 0.6	-16.0 ± 0.4	13.0 ± 0.6
351	12.4 ± 0.4	-20.2 ± 0.4	12.2 ± 0.4
475	12.5 ± 0.5	-27.5 ± 0.6	12.7 ± 0.5
588	12.1 ± 0.5	-33.5 ± 0.8	12.6 ± 0.5

D. Total nuclear cross section

The total nuclear cross section has been determined from the relation $\sigma = (4\pi/k^2)\sin^2\delta$, where δ is the fitted value of the negative s-wave nuclear phase shift at each of the five momenta studied in this experiment. These values are given in Table IV. Also given is the observed total cross section (nuclear + Coulomb) for $\cos\theta_{\text{c.m.}} \leq 0.85$.

E. Total inelastic cross section at 588 MeV/c

The threshold for $Kp \rightarrow KN\pi$ is 509 MeV/c for the incoming K^+. Events in the 588-MeV/c data sam-

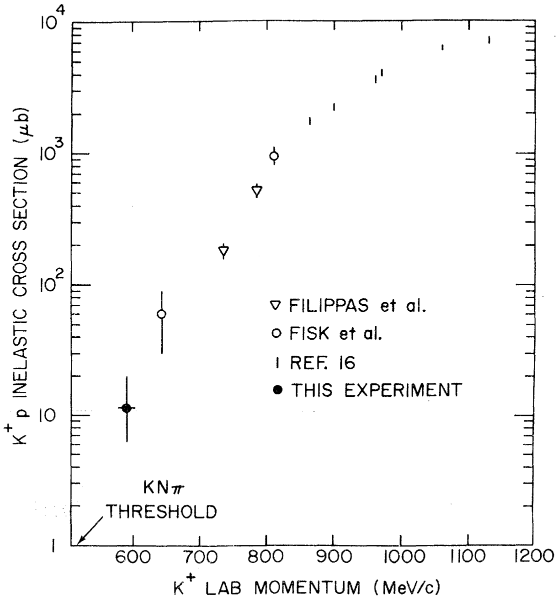

FIG. 5. The K^+p total inelastic cross section as a function of the K^+ lab momentum.

ple which did not fit the kinematic constraints of an elastic scatter were considered as candidates for inelastic scattering. Three inelastic scatters were identified on the basis of the calculated missing mass. The events were also checked on film for consistency of the observed ionization with that predicted by the one-constraint kinematic fit.

The three reactions were $K^+p \to K^+\pi^+n$ (1 event) and $K^+p \to K^0p\pi^+$ (2 events). The path length determined for the data sample which was checked for inelastics was 72.7 ± 3.1 km, giving a total inelastic cross section of 11^{+9}_{-5} μb. This value is plotted in Fig. 5 with measurements from other experiments at higher momenta.[14-16]

F. Effective-range analysis of data

We have fitted the negative s-wave phase-shift solutions to a two-parameter effective-range approximation, $k \cot\delta = 1/a + (r_0/2)k^2$, where a is the scattering length and r_0 is the effective range. We vary the parameters to minimize χ^2 and obtain the solution $a = -0.314 \pm 0.007$ F and $r_0 = 0.36 \pm 0.07$ F with a $P(\chi^2)$ of 0.52. This solution and the phase-shift data are presented in Fig. 6 plotted as $k \cot\delta$ vs k^2. The effective-range solution is a straight line with slope $r_0/2$. It is clear that r_0 is nonzero and well determined. The zero-range approximation solution gives $a = -0.345 \pm 0.004$ F, with a $P(\chi^2)$ of only 1.8×10^{-5}. These results are summarized in Table V along with the results of previous experiments.[1,17,18]

We have also used an effective-range analysis on the phase-shift solution with both s- and p-wave amplitudes. The results are shown in Fig. 3 plotted as δ vs p_{lab}. The p-wave phase shifts are small and poorly determined, so that it is sufficient to use the zero-range approximation, $\tan\delta = ak^3$, for them. The numbers obtained are $a(s_{1/2}) = -0.299 \pm 0.010$ F, $r_0(s_{1/2}) = 0.46 \pm 0.09$ F, $a(p_{1/2}) = -0.019 \pm 0.007$ F^3, and $a(p_{3/2}) = 0.010 \pm 0.004$ F^3. The $s_{1/2}$, $p_{1/2}$, and $p_{3/2}$ waves were fitted independently, giving $P(\chi^2)$ values of 0.40, 0.025, and 0.024, respectively. Analyses based on experimental data together with dispersion-theory relations have been discussed in the literature.[12,17-21]

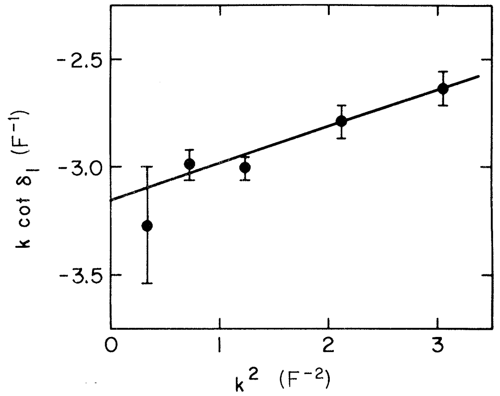

FIG. 6. A plot of $k \cot\delta_1$ vs k^2, where δ_1 is the s-wave phase shift and k is the center-of-mass wave number. The curve is the effective-range fit $k \cot\delta = a^{-1} + (r_0/2)k^2$, with $a = -0.314$ F and $r_0 = 0.36$ F.

IV. CONCLUSIONS

The measurements described in the preceding sections of the elastic scattering cross sections below 600 MeV/c including the Coulomb interference region have allowed a definite determination of the sign of the low-energy s-wave phase shifts. Our data strongly support the conclusions of Goldhaber *et al.* and others[17] that a monotonically increasing negative s-wave phase shift is the correct solution for the low-energy K^+p system. The behavior of the s-wave phase shift is fitted very well by the effective-range approximation with a nonzero effective range. We do not find any statistically significant evidence that p waves are necessary in the description of the $I = 1$ system below 600 MeV/c.

We find that there is no evidence in our data to indicate positive s-wave phase shifts as suggested by Carreras and Donnachie[3,4] on the basis of their K^+p phase-shift analysis. They obtain two solutions which involve positive s-wave phase shifts. Solution I is characterized as having a positive s-wave phase shift below 2 GeV/c. The other class of solution, Solution II, has a negative s-wave phase shift below 700 MeV/c and a positive s-wave phase shift above 700 MeV/c. We have tested these solutions as a possible description of our data at 351, 475, and 588 MeV/c. We find that the confidence levels are very low, $P(\chi^2) \ll 0.01$, for Solution I at these momenta and for Solution II at 351 and 475 MeV/c. At 588 MeV/c Solution II corresponds to the Minami ambiguity.

Figure 7 compares our K^+p total nuclear cross section measurements from Table IV with previously published measurements. The plotted curve is the cross section given by our effective-range

TABLE V. s-wave effective-range analyses of low-energy K^+p scattering.

a (10^{-13} cm)	r_0 (10^{-13} cm)	$P(\chi^2)$	Reference
-0.345 ± 0.004	0 (fixed)	1.8×10^{-5}	This experiment
-0.314 ± 0.007	0.36 ± 0.07	0.52	This experiment
-0.33 ± 0.01	0 (fixed)	0.01	Ref. 1
-0.29 ± 0.015	0.5 ± 0.15	0.85	Ref. 1
-0.2981 ± 0.0016	0.434 ± 0.014	···	Refs. 17,18

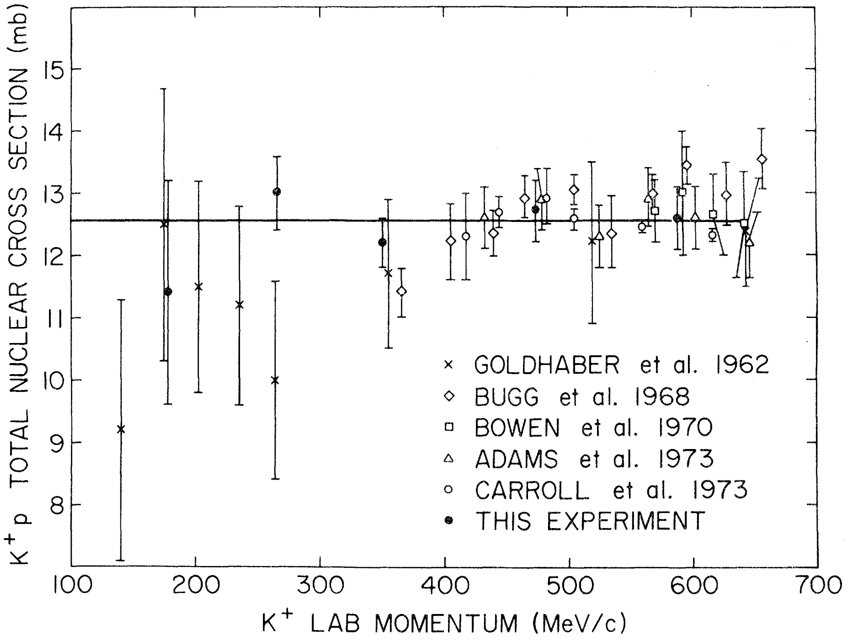

FIG. 7. The K^+p total cross section. The other experiments are from Refs. 17, 18, and 22–25. The curve is our s-wave effective-range fit.

analysis with negative s-wave phase shifts. Our results agree with the previous bubble-chamber experiment of Goldhaber *et al.*[1] and some recent counter experiments.[17,18,22-25]

The inelastic cross section at 588 MeV/c is closer to the inelastic threshold than any other result. It is too large to be explained by a simple Breit-Wigner extrapolation of the $K^*(890)$ from higher energies.

When this work was essentially completed, we received a preprint of similar work by Cameron *et al.*[26] Their results are in good agreement with ours.

ACKNOWLEDGMENTS

We would like to thank Dr. V. R. Veirs, Mr. J. Wallace, and Mr. D. Trevvett for their valuable assistance in early phases of this work. We also wish to acknowledge the efforts of the many members of the bubble-chamber groups at Maryland and IIT, especially Mr. C. Aaron, Ms. E. Dann, Ms. M. Kocik, Ms. G. Parks, and Mr. R. Petri.

---

*Work supported in part by U. S. Atomic Energy Commission and by the National Science Foundation.

†Present address: Finn & Fram, Inc., 8400 San Fernando Road, Sun Valley, California 91352.

[1] S. Goldhaber *et al.*, Phys. Rev. Lett. 9, 135 (1962).

[2] T. F. Kycia, L. T. Kerth, and R. G. Baender, Phys. Rev. 118, 553 (1960).

[3] B. Carreras, A. Donnachie, and R. Kirsopp, in *Hyperon Resonances—70*, edited by Earle C. Fowler (Moore, Durham, N.C., 1970), p. 447.

[4] B. Carreras and A. Donnachie, Nucl. Phys. B23, 525 (1970); Daresbury Report No. 37, 1971 (unpublished).

[5] J. D. Jackson and J. M. Blatt, Rev. Mod. Phys. 22, 77 (1950); M. L. Goldberger and K. M. Watson, *Collision Theory* (Wiley, New York, 1964).

[6] Further experimental details may be found in the Ph.D. thesis of J. R. Fram, University of Maryland Technical Report No. 74-070, 1973 (unpublished).

[7] D. Berley, Brookhaven National Laboratory AGS Internal Report No. DB-1, 1963 (unpublished).

[8] The automatic film measuring machine PEPR was used at the University of Maryland to measure elastic scatters at 178, 265, and 351 MeV/c. The PEPR system uses the standard astrodata hardware with a PDP-10 48 K computer. The software evolved from the Argonne National Laboratory POLLY ststem. The track-following strategy used the local properties of tracks to the maximum possible extent, since this low-energy film had many steep highly curved tracks. The system was used in an operator-controlled mode which allowed the operator to intervene and direct the automatic track-measuring procedure when necessary. The results of the PEPR measurements are comparable to manual measurements in precision, and reflect a more rapid measurement rate. This experiment was the first application of the University by Maryland PEPR system.

Further details can be found in R. G. Glasser and G. E. McClellan, in *Proceedings of the Oxford Conference on Computer Scanning*, Vol. I, edited by P. G. Davey and B. M. Hawes (Oxford Univ. Press, Oxford, 1974), p. 61.

[9] T. B. Day, University of Maryland Technical Report No. 649, 1966 (unpublished).

[10] Particle Data Group, Rev. Mod. Phys. 45, S1 (1973).

[11] F. T. Solmitz, Phys. Rev. 94, 1799 (1954).

[12] C. P. Knudsen and B. R. Martin, Nucl. Phys. B61, 307 (1973).

[13] M. G. Albrow, S. Andersson/Almehed, B. Bošnjaković, C. Daum, F. C. Erné, Y. Kimura, J. P. Lagnaux, J. T. Sens, F. Udo, and F. Wagner, Nucl. Phys. B30, 273 (1971).

[14] J. Fisk, H. K. Ticho, D. H. Stork, W. Chinowsky, G. Goldhaber, S. Goldhaber, and T. F. Stubbs, in *Proceedings of the 1962 International Conference on High-Energy Physics at CERN*, edited by J. Prentki (CERN, Geneva 1962), p. 358.

[15] T. A. Filippas, V. P. Henri, B. Jongejans, M. Krammer, J. M. Perreau, S. Focardi, A. Minguzzi-Ranzi, L. Monari, G. Saltini, P. Serra, E. Barrelet, E. Huffer, and F. Muller, Nuovo Cimento 51A, 1053 (1967).

[16] The unlabeled points of Fig. 5 were taken from E. Bracci, J. P. Droulez, E. Flaminio, J. D. Hansen, and D. R. O. Morrison, CERN/HERA Report No. 72-2, 1972 (unpublished).

[17] C. J. Adams, J. D. Davies, J. D. Dowell, G. H. Grayer, P. M. Hattersley, R. J. Howells, C. McLeod, T. F. McMahon, H. B. van der Raay, L. Rob, C. J. S. Damerell, R. J. Homer, and M. J. Hotchkiss, Phys. Rev. D 4, 2637 (1971); and Rutherford Laboratory Report No. 73-071, 1973 (unpublished).

[18] C. J. Adams, G. F. Cox, J. D. Davies, J. D. Dowell, G. H. Grayer, P. M. Hattersley, R. J. Howells, C. McLeod, T. J. McMahon, H. B. van der Raay, L. Rob, C. J. S. Damerell, and M. J. Hotchkiss, Nucl. Phys. B66, 36 (1973); J. D. Dowell, in *Proceedings of the XVI International Conference on High Energy Physics, Chicago-Batavia, Ill., 1972,* edited by J. D. Jackson and A. Roberts (NAL, Batavia, Ill., 1973), Vol. 1, p. 40; in *Proceedings of the Purdue Conference on Baryon Resonances* (Purdue Univ., Lafayette, Ind., 1973), p. 157.

[19] A. D. Martin and R. Perrin, Nucl. Phys. B10, 125 (1969).

[20] G. K. Oades (editor), Rutherford Laboratory Report No. RHEL/R245, 1972 (unpublished).

[21] R. E. Cutkosky and B. B. Deo, Phys. Rev. D 1, 2547 (1970).

[22] D. V. Bugg, R. S. Gilmore, K. M. Knight, D. C. Salter, G. H. Stafford, E. J. N. Wilson, J. D. Davies, J. D. Dowell, P. M. Hattersley, R. J. Homer, A. W. O'Dell, A. A. Carter, R. J. Tapper, and K. F. Riley, Phys. Rev. 168, 1466 (1968).

[23] T. Bowen, P. K. Caldwell, F. N. Dikmen, E. W. Jenkins, R. M. Kalbach, D. V. Petersen, and A. E. Pifer, Phys. Rev. D 2, 2599 (1970).

[24] T. Bowen, E. W. Jenkins, R. M. Kalbach, D. V. Petersen, A. F. Pifer, and P. K. Caldwell, Phys. Rev. D 7, 22 (1973).

[25] A. S. Carroll, T. F. Kycia, K. K. Li, D. N. Michael, P. M. Mockett, D. C. Rahm, and R. Rubenstein, Phys. Lett. 45B, 531 (1973); A. S. Carroll (private communication).

[26] W. Cameron, A. A. Hirata, R. Jennings, W. T. Morton, E. Cazzoli, G. Giacomelli, P. Lugaresi-Serra, G. Mandrioli, A. Minguzzi-Ranzi, E. Castelli, M. Furlan, P. Poropat, C. Omero, and M. Sessa, Nucl. Phys. B78, 93 (1974).